Bachelor Thesis

Uncertainty in Graph Neural Networks, applied within Quantum Chemistry

Name:	**Student number:**
Lars Lohmann	s173875

Supervisor:	**Title:**
Mikkel Nørgaard Schmidt	Associate Professor

Department:

Department of Applied Mathematics and Computer Science, Technical University of Denmark

1 Abstract

Contents

2 Acknowledgements

The completion of this project would not have been possible without the dedicated supervisor efforts from Mikkel Nørgaard Schmidt.

Mikkel Nørgaard Schmidts help has manifested through all of the stages of the project, from planning, to scoping, to executing and finalizing. His inviting presence allows for curiosity to an extend very few prior of prior supervisors have managed. His own curiosity towards the topic is contagious. His on the spot questioning and advice, has contributed to the bettering of the project, and a deepening of the knowledge around the subject matter.

When things get tough, his calming manner gave the mental surplus that was needed to finalize the work, and deliver on this project.

I would recommend his counselling efforts to any student at DTU, whether it being in a project or in a teaching capacity.

Thank you!

Lars Lohmann - s173875

3 Introduction

The implications of predicting molecular properties and dynamics have both large industrial- and research implications within the natural- and life-sciences. The large amounts of compute, necessary for simulation, often makes desirable metrics intractable to estimate. The efforts of this study, will help provide tools for industry to reduce lead time and risk in development fields such as drug discovery and material sciences for energy storage[1].

These interests, have for many years been supported by research and development methods within the traditional field of chemistry, with emphasis on estimation techniques, that carry a heavy computational load like traditional molecular dynamics (MD)[2] or Density Functional Theory[1]. Therefore, despite the emergence of cloud-data-centers and power full algorithms available at lower cost to research, some problems still exist which are intractable with known methods.

That fact, has prompted the emergence of the computational fields within Artificial Intelligence (AI), such as Machine Learning (ML), Deep Learning (DL) and Geometric Deep Learning (GDL), to enrich the solution space. These methods produce models which tries to decrease the lead time for predictions, while maintaining an acceptable error-rate[3]. Specifically the field of Geometric Deep Learning, has emerged with a viable set of data-driven methods, for predicting molecular properties and dynamics[4]. Geometric Deep Learning comprises a set of methods, which tries to enrich the initial data structures with a geometric prior. One of these methods is graph neural networks (GNN's) which structures the molecular-data in graphs, which is comprised of nodes and edges between nodes (representing atoms and bonds respectively), in an i.e euclidean space[4]. These models can encode information such as distances, angles or directions between nodes, allowing also for symmetry-priors of the invariant and equivariant types[5]
The most popular architecture within GNN's is the Message Passing Neural Network (MPNN)[4]. This architecture, allows for iterative updates of message information between nodes in the graph representation, allowing for exchanges of information between nodes based on their relationship to each other. Specific models that have shown promise within the chemical space, is the Directional Message Passing Neural Network (DimeNet) model[3], the Multiplex Molecular Graph Neural Network (MXMNet) model [6], and the polarizable atom interaction neural network (PAINN) model[7]. Central to these models is the graph representation of information, allowing for node-features to update based on the information of neighbouring nodes. Where they differ is in i.e their definition of the term neighbour. Traditionally, the concept of a neighbour node, is mainly defined by the euclidean distance between the nodes[8]. This however, DimeNet challenges by including directional information in the definition, while maintaining critical symmetry properties in the model. MXMNet segments node representations into two segments, those representing a covalent influence on the node, and those representing a Wan der Waals influence on the node, allowing them to be modeled seperately and weighed based on importance[6]. In

the case of the PAINN-model, it introduces novel ways to do equivariant operations in cartesian space, allowing the model achitecture to outperform among other the DimeNet model, on numerousprediction tasks.

Since significant risk is embodied in the task of predicting chemical and biochemical dynamics, due to end-uses often being utilized in pharmaceutical products, proper mechanisms for estimating the the uncertainty around prediction methods, and mitigating the impact of high uncertainty through calibration, are needed. Traditionally, data-driven methods within machine learning and deep learning, have problems with providing the necessary uncertainties, on the metrics being predicted, making calibration for more robust overall performance hard[9][1][10]. Providing methods for estimating uncertainty, and calibrating, would allow for defaulting to more traditional methods for estimating chemical properties, when uncertainty is high in the data-driven models[1].

In support of producing such methods, uncertainty, can effectively be distinguished between two concepts, namely epistemic- and aleatoric- uncertainty[1][10]. Aleatoric, also known as statistical uncertainty, refers to the uncertainty inherent in experimental outcomes, due to random effects. This class of uncertainty is classified as irreducible, due to no amount of additional information in the modelling effort, being able to reduce this type of uncertainty[10]. Epistemic, also called systemic uncertainty, refers to the uncertainty in a model, produced by lack of information, and can therefore be reduced. These two elements of uncertainty are considered by researchers to be the sole components of total uncertainty, their sum being equal to total uncertainty in an experiment[10]. Specific methods for estimating these classes of uncertainty in neural networks, have been proposed in recent years. In [11], Three methods for estimating uncertainty for in Deep Neural Networks (DNN's). These three methods are Monte Carlo Dropout (MC Dropout), Ensembling, and Bootstrapping. MC Dropout, relies on training neural networks (NN's), with dropout regularization, and after training producing a set of samples, with different random masks. The uncertainty can then be estimate by looking at the variance over these predictions. Ensembling relies on training the same model architecture, on the same data set with random initializations. The uncertainty can then be estimated by looking at the variance of the predictions of the ensemble of models. Evidence suggests that these ensembles produce better results, when the ensemble is 'diverse'[12]. These recent results indicate implementing methods like early stopping (A method that breaks the training-loop if a validation metric stagnates), and weight decay (A method that penalises large weights in the neural network), will increase this diversity for the better. These methods applied to ensembling, is viewed as a discrete method from ensembling itself[11] called anchored ensembling. Similar to ensembling is bootstrapping, where a set of models are trained like in ensembling, but this time of different subsets of the data set. These subsets are picked with replacement at random, and all subsets will effectively have some overlap in data points, while still having some diversity in points among each other. The conclusion in [11] is that bootstrapping and ensembling are both superior methods to MC Dropout, while being inconclusive on which is the better method

between bootstrapping and ensembling.

The overall goal of this project, is to compare two ensembles of five machine learning models in each, which all are of the type Message Passing Neural Networks with architecture inspired by the PAINN architecture[7]. PAINN has been established as a state of the art method, within the space of GNN's in the field of chemistry, which was essential for the choice of the architecture. The individual models in the ensemble, output a single metric, trying to predict the binding energy of the catalyst process represented by its input. These predictions are then combined to produce a mean prediction and a variance for each ensemble. although the individual models are similar in architecture, they have different hyperparameters in their internal representations of molecules. Specifically the state representation of scalar- and vector-properties of the input graphs. One ensemble of models will have a half (64) of the dimensions-size for representing both scalar- and vector-properties, compared to the other ensemble (128). The individual models in the ensembles will be trained with weight decay and early stopping, in alignment with current state of the art methods, in order to produce diversity.

The models will be trained on a molecular data set[13], comprising of 7.053 molecules. This dataset contain atom-types, coordinates, and binding energy in kcal per mol, where the latter is our regression target. The main contribution of this paper, will be to assess the influence of this hyperparameter difference on modelling performance measured by the mean squared error (MSE) between the predictions of the ensembles and the actual target values, and epistemic uncertainty founded in the variance in the predictions of the ensembles inspired by[14], and [15]. The Expected Normalized Calibration Error (ENCE), will also be calculated as a supplementary measure.

The goal of this project has been to implement the model architecture from scratch, utilizing tools and packages from the *PyTorch* library. This with the intention of achieving a more detailed understanding of the modelling task, uncertainty in modelling, and the model structure itself. This specifically means implementing the MPNN architecture[7], and the ensembling procedure from scratch. The project is limited in terms of providing a measure for both epistemic and aleatoric uncertainty. Since the individual models in the ensembles only predict a single value, trying to minimize the MSE-loss function, and not an output mean and variance like done in Busk2021[1], and proposed in [14], aleatoric uncertainty can not be estimated. The distinquishing between the two types of uncertainty, while being the state of the art for evaluating uncertainty in modelling tasks, is not attainable due to the scope of the project. The choice of estimating uncertainty via the variance and mean over ensemble predictions, are viable options performed in Tran[15], and proposed by Scalia[11], but critiqued for its lack of capabilities in Lakshminarayanan[14]. The sole data set in scope of this project is the C-c catalyst dataset[13]. The choice came down to the accesability of the data set, being limited to 7.053 molecules, with easy to comprehend data structures. This choice supported the desire to emphasize understanding the modelling task and uncertainty in modelling.

Specifically, this paper asks:

Does the size of internal state representations, impact prediction error and uncertainty in ensembles of Message Passing Neural Networks

The following sections of this paper, namely[3,4], we will go through relevant concepts and theories, necessary for assessing the results and methods in this paper. This is followed by a description of the experimental methods, and a presentation of the data set, on which the methods have been utilized in sections[5,6]. Lastly, results followed by a conclusion and a discussion of the potential points of error, which influence the outcomes of the experiment in sections[7,8,9].

4 Theory

In this section, we will discuss the theoretical foundations of message passing neural networks (MPNNs) and ensembles for predicting the binding energy of molecules in a catalyst process.

4.1 Message Passing Neural Networks

The key idea behind MPNNs is the concept of message passing, where each node in the graph exchanges information with its neighbors in an iterative manner.
Let $G = (N, E)$ be a graph, where N is the set of nodes and E is the set of edges. Each node $n \in N$ is associated with an invariant representation vector $\mathbf{S}_n \in \mathbb{R}^{Fx1}$, an equivariant representation vector $\vec{\mathbf{v}}_n \in \mathbb{R}^{Fx3}$ and a position in 3D space $\vec{r}_i \in \mathbb{R}^3$. F denotes the number of features in the state representation (in our case, $F = 64$ and $F = 128$). Each edge $(i, j) \in E$ is associated with a relative position $\vec{r}_{ij} = \vec{r}_i - \vec{r}_j$. A node $n_j \in N$ is said to be a neighbour of a node $n_i \in N \setminus \{n_j\} = \mathscr{N}(i)$ if n_j is within the cutoff distance of n_i: $\mathscr{N}(i) = \{j | \|\vec{r}_{ij}\| \leq r_{cut}\}$.
The message passing process in an MPNN can be described by the following equations 1 and 2 following the notation of [7].

$$\vec{\mathbf{m}}_i^{v,t+1} = \sum_{j \in \mathscr{N}(i)} \vec{M}_t(\mathbf{S}_i^t, \mathbf{S}_j^t, \vec{\mathbf{v}}_i^t, \vec{\mathbf{v}}_j^t, \vec{r}_{ij}) \tag{1}$$

$$\vec{\mathbf{s}}_i^{v,t+1} = \vec{U}_t(\mathbf{S}_i^t, \vec{\mathbf{v}}_i^t, \vec{\mathbf{m}}_i^{v,t+1}) \tag{2}$$

The U and M functions respectively being the update, and message functions, taking into account scalar, vector and directional features. These equations utilize both invariant and equivariant representations, letting representations interact, in accordance with knowledge surrounding the chemical descriptor trying to be predicted. The underlying operations of the functions U and M, have a linearity constraint on equivariant representations of directional information, in order to maintain information, throughout the modelling process[4].
Further, we define the residual update of invariant scalar3-representations in the message block:

$$\Delta \mathbf{s}_i^m = (\phi_s(\mathbf{s}) * \mathscr{W}_s)_i = \sum_j \phi_s(\mathbf{s}) \circ \mathscr{W}_s\left(\left\|r_{ij}\right\|\right) \tag{3}$$

Worht mentioning about the above expression, are that the index 's' refers to a certain split of the $\phi \circ W$-product seen in figure2. All indexes in the below equations, whether belonging to the message block or the update block, will have indexes detailing what part of a split it belongs to being either 's', 'v' or a combination of the two. In the above equation, two expression are utilized, namely ϕ_s and $\mathscr{W}_s$. ϕ_s represents atomwwise layers, which have undergone transformations through two linear layers and a SiLU-function, introducing some non-linearity potentially for better gradient flow, via the smooth gradient. Conceptually it can be interpreted as an expansion of the embedded atomwise neighbours of a node. Let $f(x)$ denote a linear layer:

$$f(x) = w \cdot x + b \tag{4}$$

and $SiLU(x)$ denote the SiLU-function:

$$SiLU(x) = x \cdot \left(\frac{1}{(1+e^{-x}))} \right) \tag{5}$$

Then ϕ is defined as:

$$\phi_s(\mathbf{s}) = f(SiLU(f(\mathbf{s}))) \tag{6}$$

The rotationally invariant filters $\mathscr{W}_s$ are defined as, are linear combinations of a radial basis function (RBF)15[4]. The radial basis function outputs are chosen such that it is centered around twenty points, $C = \{1, 2, 3, \ldots, 20\}$. These twenty points are centers of the filter, and their units are Angstrom. These centers are chosen, such that they cover all distances in the data set, which is confirmed in a later section9. The expansions provide a representation of similarity or dissimilarity, between the input relative position $\vec{r}_{ij}$, and the chosen points C [16]. The function takes directional information $\|\vec{r}_{ij}\|$ and a cutoff r_{cut}. The rbf acts as filter generating function[17], effectively quantizing the directional information. The function is defined as:

$$\mathbf{RBF}(\|\vec{r}_{ij}\|) = \sin\left(\frac{C\pi}{r_{cut}} \cdot \|\vec{r}_{ij}\| \right) / \|\vec{r}_{ij}\| \tag{7}$$

This radial basis is then expanded on by a linear layer f, before the cosine cutoff function is applied. This effectively means that, that atoms beyond the cutoff radius, does not contribute to the representation[2]. The cosine cutoff function is defined as:

$$\mathbf{f}_{cut}(\|\vec{r}_{ij}\|) = \begin{cases} 0.5 \cdot \cos\left(\frac{\pi \|\vec{r}_{ij}\|}{r_{cut}} + 1 \right) \cdot f(\mathbf{RBF}(\|\vec{r}_{ij}\|)) & \text{if } d \leq r_{cut} \\ 0 & \text{if } d > r_{cut} \end{cases} \tag{8}$$

Worth mentioning is that the cosine cutoff implemented in this project, has an added factor compared to Behler2011[2], namely $f(\mathbf{RBF}(\|\vec{r}_{ij}\|))$. This is deemed missing by the project, and is therefore added. The full representation of the rotationally invariant filters are therefore:

$$\mathscr{W}_s = \mathbf{f}_{cut}(\|\vec{r}_{ij}\|, f(\mathbf{RBF}(\|\vec{r}_{ij}\|)) \tag{9}$$

Next also utilizing continous-filter convolutions $\mathscr{W}$, we define the residual equivariant vector update as:

$$\Delta\vec{\mathbf{v}}_i^m = \sum_j \vec{\mathbf{v}}_j \circ \phi_{vv}(\mathbf{s}_j) \circ \mathscr{W}_{vv}\left(\left\| \vec{\mathbf{r}}_{ij} \right\| \right) + \sum_j \phi_{vs}(\mathbf{s}_j) \circ \mathscr{W}'_{vs}\left(\left\| \vec{\mathbf{r}}_{ij} \right\| \right) * \frac{\vec{\mathbf{r}}_{ij}}{\left\| \vec{\mathbf{r}}_{ij} \right\|} \tag{10}$$

The equation10 consists of two terms. The first being a convolution of an invariant filter
As well as the residual update of equivariant vector-representations in the message-10 and update-block12 as:

$$\Delta\mathbf{s}_i^u = \mathbf{a}_{ss}\left(\mathbf{s}_i, \|\mathbf{V}\vec{\mathbf{v}}_i\|\right) + \mathbf{a}_{sv}\left(\mathbf{s}_i, \|\mathbf{V}\vec{\mathbf{v}}_i\|\right) \langle \mathbf{U}\vec{\mathbf{v}}_i, \mathbf{V}\vec{\mathbf{v}}_i \rangle \tag{11}$$

$$\Delta\mathbf{v}_i^u = \mathbf{a}_{vv}\left(\mathbf{s}_i, \|\mathbf{V}\vec{\mathbf{v}}_i\|\right) \mathbf{U}\vec{\mathbf{v}}_i \tag{12}$$

These operations need to be chosen, such that they fullfill either of the two equations (13 for invariant representations or 14 for equivariant representations) as shown below for any rotation matrix $R \in \mathbb{R}^{3\times3}$:

$$\mathbf{f}(\vec{\mathbf{x}}) = \mathbf{f}(R\vec{\mathbf{x}}) \tag{13}$$

$$R\vec{\mathbf{f}}(\vec{\mathbf{x}}) = \mathbf{f}(R\vec{\mathbf{x}}) \tag{14}$$

The paper of inspiration [7] highlights a list of operations, that MPNN's in particular can use:

- Any (nonlinear) function of scalars: $\mathbf{f}(\mathbf{s})$
- Scaling of vectors $\mathbf{s} \circ \vec{\mathbf{v}}$
- Linear combinations of equivariant vectors: $\mathbf{W}\vec{\mathbf{v}}$
- Scalar products: $\mathbf{s} = \|\vec{\mathbf{v}}\|^2, s = \langle \vec{\mathbf{v}}_1, \vec{\mathbf{v}}_2 \rangle$
- Vector products: $\vec{\mathbf{v}}_1 \times \vec{\mathbf{v}}_2$

If we look at the residual updates of the scalar- and vector-representations, in the message- and update block.

Figure 1: Message Block

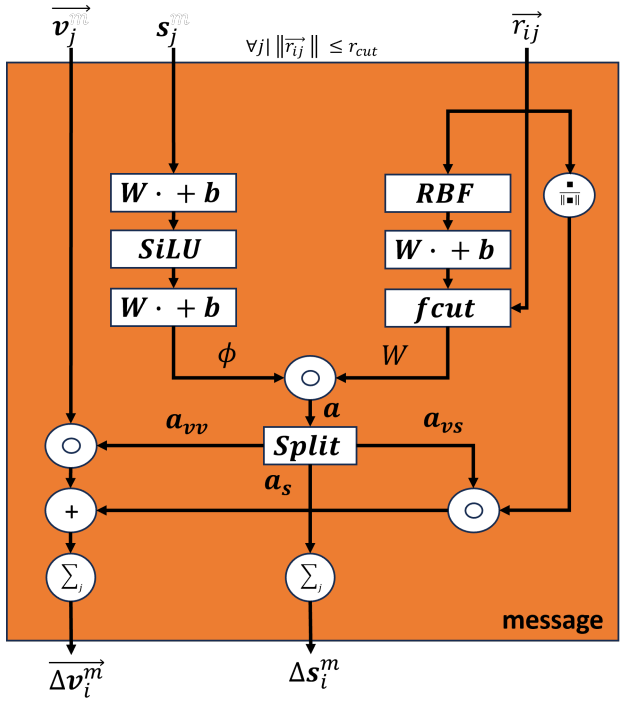

Equivariant representations of directions between nodes, have shown to be more expressive, at a similar computational cost. This compared to rotationally invariant representations of either angular- or distance information This effectively means a higher level of information can be maintained through the modelling phase, if the equivariance is maintained.

Directional information is also expanded from the relative positions between edges $\vec{r}_{ij}$, via the radial basis function (RBF)[4].The radial basis function outputs are chosen such that it is centered around twenty points, $C = \{1,2,3,\ldots,20\}$. The function takes directional information $d = \|\vec{r}_{ij}\|$ and a cutoff r_{cut}, and produces expansions following the formula below.

$$\mathbf{RBF}(d) = \sum_{c \in C} \sin\left(\frac{c\pi}{r_{cut}} * d\right)/d \tag{15}$$

The expansions provides a representation of similarity or dissimilarity, between the input relative position $\vec{r}_{ij}$, and the chosen points C [16]. This information is further expanded by a neural network layer with a set of weights biases, seen in equation 16, before arriving at the cosine cutoff.

$$y_{rbf} = \mathbf{w} \cdot \mathbf{RBF}(d) + \mathbf{b} \tag{16}$$

The cosine-cutoff function is originally derived from [2] in the form of the equation below17.

$$\mathbf{f}_{cut}(x) = \begin{cases} 0.5 \cdot \cos\left(\frac{\pi d}{r_{cut}} + 1\right) & \text{if } d \leq r_{cut} \\ 0 & \text{if } d > r_{cut} \end{cases} \tag{17}$$

The cutoff function implemented in this project, utilized the equation below18:

$$\mathbf{f}_{cut}(x) = \begin{cases} 0.5 \cdot \cos\left(\frac{\pi d}{r_{cut}} + 1\right) \cdot y_{rbf} & \text{if } d \leq r_{cut} \\ 0 & \text{if } d > r_{cut} \end{cases} \tag{18}$$

This alteration allows for the flow of information from both the radial basis expansions and the initial vector differences, which from the process diagram in[7], is not happening, although this is believed by the project to be the intention. These three highlighted steps, the rbf, the set of weights and biases and the cosine cutoff, constitute the rotationally invariant filter $\mathscr{W}_s$, proposed by [3], and [2], and have been highlighted in this section, due to the difference in approaches from these propositions.

4.2 Ensembles

Ensembles is a technique for combining the predictive performance of individual modelling approaches and to as an extension measuring total uncertainty in the model. In the context of MPNNs, ensembles can be created by training multiple models with different initializations, and combining their predictions.

Let $\mathbf{y}_i$ be the predicted binding energy for molecule i by model M_k, where i represents the molecule index and k represents the model index. The ensemble prediction $\hat{\mathbf{y}}_i$ can be calculated as the mean of the individual model predictions, as done in[15]:

$$\hat{\mathbf{y}}_i = \frac{1}{T}\sum_{k=1}^{T} \mathbf{y}_i^{(j)} = \hat{\mu}_i \tag{19}$$

where T is the number of models in the ensemble. This format of calculation weights the inputs from each model equally, similarly to if it was a uniformly weighted mixture model as in [1].

To estimate the uncertainty in the ensemble predictions, we can calculate the variance of the individual model predictions[15]:

$$\text{Var}(\hat{\mathbf{y}}_i) = \frac{1}{T}\sum_{k=1}^{T}(\mathbf{y}_i^{(k)} - \hat{\mathbf{y}}_i)^2 = \hat{\sigma_i^2} \tag{20}$$

Finally as the foundation of estimating uncertainty in the ensemble predictions, we can estimate the expected normal calibration error. This method relies on sorting predictions of targets, in K equal sized bins, computing the predicted root mean variance21.

$$RMV_k = ? \tag{21}$$

Thereafter producing the empirical root mean squared error22:

$$RMSE_k = \sqrt{\frac{1}{k}\sum_{k=1}^{K}\left(\mathbf{y}_i^{(k)} - \hat{\mathbf{y}}_i\right)^2} \tag{22}$$

and finally utilizing the expression, following equation the equation in[1]:

$$ENCE = \frac{1}{k}\sum_{k=1}^{K}\frac{|RMV_k - RMSE_k|}{RMV_k} \tag{23}$$

The approach of [1] is based on models in an ensemble, outputting both a mean value and a variance metric, effectively predicting both the target, and predicting its own uncertainty. This is not the case in this project, since the model solely predicts the target.

4.3 Model

The model architecture consists of two main components, namely the Message block, and the Update block as formerly introduced in the the theory section 1, and 2. The Message block is conceptually responsible for the message passing between the nodes in the graph, allowing for the flow of information between the nodes. This information is then summed up and stored in state variables in the form of a scalar and vector representation. This summation is done in a residual manner, following the implementation of the PAINN architecture[7]. An equation defining the residual calculation of the scalar-properties3 and vector-properties10 can be found below, as well as an illustration of the message block2.

Figure 2: Message Block

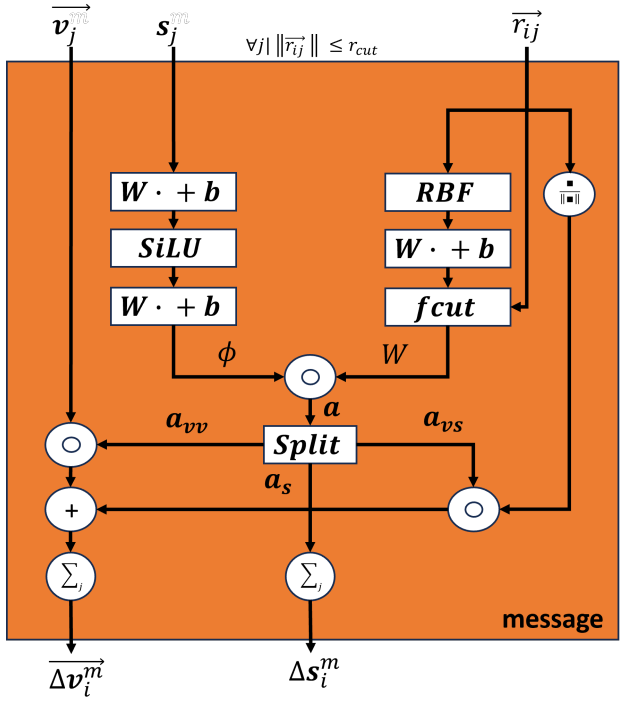

Worth noting about the figure, compared to the similar one in [7], is the use of the *r_ij* vector, that also flow into the 'fcut' function, as mentioned in 4.1. The model in this paper, does not highlight the dimension expansions or collisions from network element to network element, due to the model parameters varying in size, as it is the scope of this project to investigate similarities or dissimilarities in performance, with respect to the PAINN architecture and dissimilar state representation sizes. both sizes ϕ and $\mathscr{W}$ are chosen sub-architectures based on the PAINN architecture from[7]. The image also contains hints of the $\mathbf{a}$-tensor, which is a product of the ϕ and $\mathscr{W}$ tensors, and not highlighted in [7].

The residual values produced in the message block, then used in the update block, in order to update the node states, based on the summation over neighbouring states. This structure is also heavily inspired by the PAINN architecture[7]. The below equations represent the residual updates on both the scalar- 11 and the vector- 12 properties. Below is also a figure representing the update block3.

Figure 3: Update block

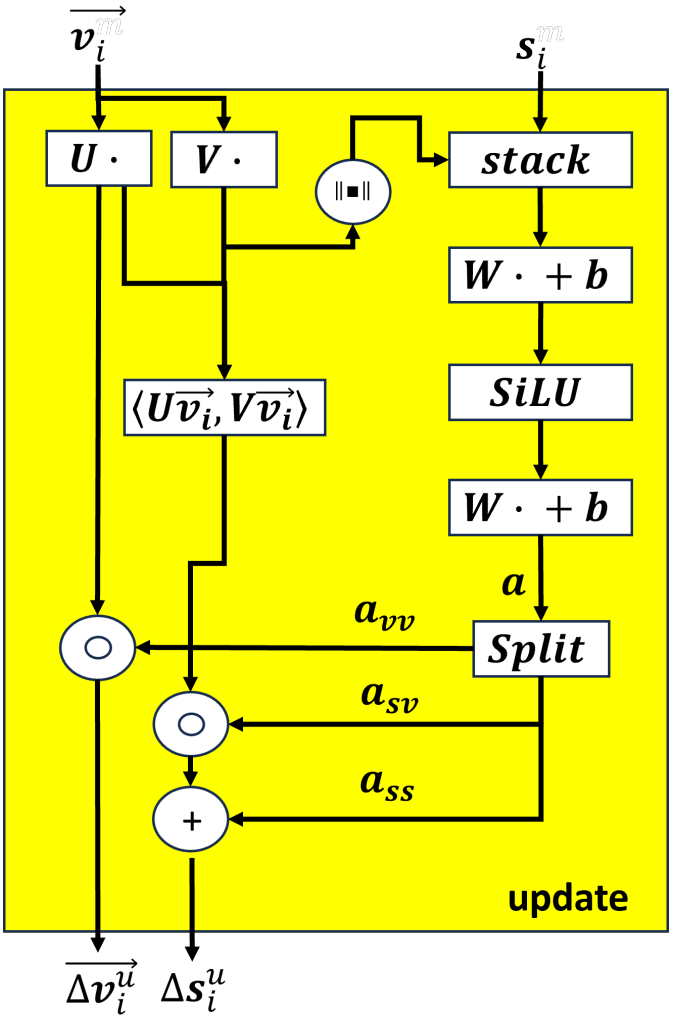

Worth noting about the above figure 3, is that the indexes of the scalar and vector representations, have been altered, compared to [7]. This comes down to the project evaluating the indexing of the scalar and vector representations, in the paper, were faulty, and did not represent the PAINN architecture as described in prior sections of the paper.

The blocks are stacked in coupled sequences of five full rounds, like the illustration below highlights4, a corresponsding model can be found in [7]. The illustration shows an architecture comprised of three sets of message- and update-blocks, the implementation in this project utilized five sets. The model representation property $\vec{v}_i^0$ is initialized to the zero vector, and the scalar property S_i^0 is initialized to a random embedding on atom level, for each node in the graph.

Figure 4: MPNN Full Architecture

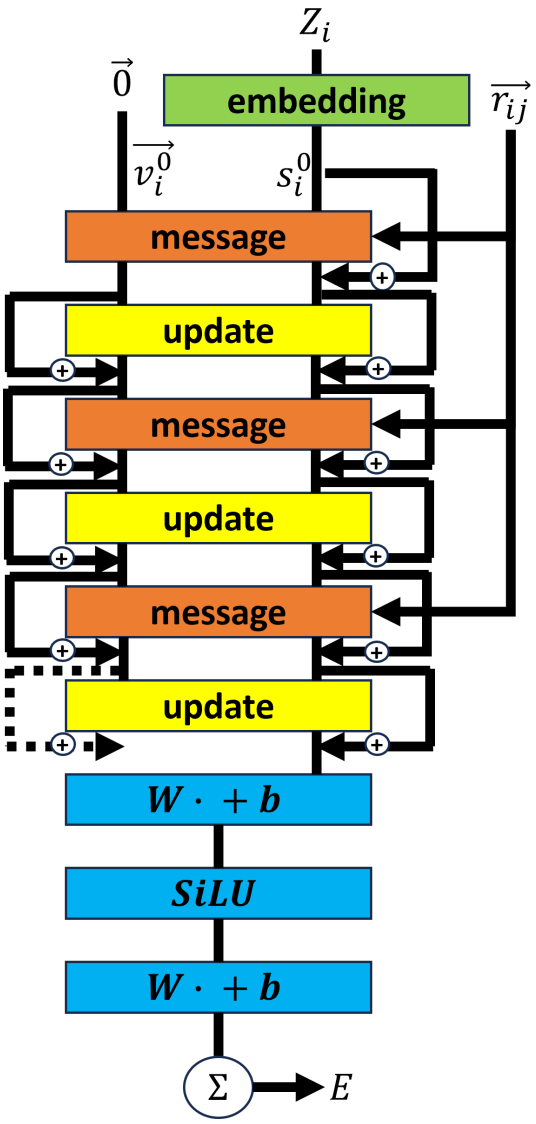

5 Methods

This section will detail the implementation and necessary technological foundation, for applying the theories described, in order to produce the experimental results for answering the research question. The section will also detail the necessary information, for reproducing and understading the experimental results and their becoming.

5.1 Experimental Setup

The experimental setup are comprised of the following components:

- Dataset
- Model
- Training- and Validation-Loop
- Test loop

These four components all together make up the main functionality of the experiment, and will be detailed individually below. The detailing will have its focus on how concepts and theories previously explained, are formatted and shaped, in order to be viable for practical modelling purposes.

5.2 Dataset

The data set is comprised of one row for each node for 695 molecules, with a the following fields for each node:

- Atom-type
- Overall binding energy (target property)
- x-coordinate
- y-coordinate
- z-coordinate
- Graph id

The atom type signifies the type of atom for a given node by name. The overall binding energy is the target property, for the full catalyst process. This means all nodes with identical graph id will have a identical overall binding energy. The x, y, and z coordinates are the coordinates of the nodes in the molecular graph, measured in Ångstrøm.
These fields are then translated to the relevant datastructures, via the graph data set constructor. This constructor defines the following data structures, for utilization in the modelling task. Important to say is that the data set constructor, constructs a data set of popentially several graphs, and not only one. The data set consists of the following critical fields:

- num_nodes: Number of nodes in the data set of graphs
- node_from: The node from which the edge originates
- node_to: The node to which the edge points
- num_graphs: Number of graphs in the data set
- node_graph_index: The index of the graph the edge resides in
- unique_atoms: The number of unique atoms in the data set
- edge_lengths: The lengths of the edges
- edge_vector_diffs: The vector differences of the edges

The number of nodes in dataset, allows for the model to create initial state representation structures with proper dimensions for the modelling task. The node_from property, allows for summation of all neighbouring node state representations, within the cutoff limit, into the designated node, we are trying to model in the message block. The node_to property, allows for initialising the state representation of the node in the update block, namely the scalar properties and the vector properties. The scalar properties are concatenated tensors of embedded atom representations, linked by the index in the node_to property. For scalar properties it is zero-vectors, instead of embedded tensors. The num_graphs property is used to initalize the initial state representation of the graphs. The node_graph_index property is an index linking an edge, to a corresponding graph. When summing over all neighbour nodes occur, the full message state representation of all neighbours under the cutoff, is summed over the node_graph_index property, to produce a state representation of graphs. The unique_atoms property, allows for the embedding function to create a unique atom representation for each type of atom in the data set. The edge_lengths allow for a masking of the edges and thereby nodes that are not within the cutoff limit. The edge_vector_diffs are the vector differences of the edges, being an input variable in the message block.

5.3 Training- and Validation-loop

Algorithm 1 MPNN Training Loop

Initialize size of ensemble: T
Initialize size of batch: B
Initialize data sets: Td, Vd
initialize training data loader: $TD = Dataloader(B, Td)$
initialize validation data loader: $VD = Dataloader(B, Vd)$
Initialize number of epochs: E
Initialize validation index: V
for $model = 1, 2, \ldots, T$ **do**
    Initialize MPNN model instance: $model = PAINN()$
    initialize MSE loss function: $loss = MSE()$
    Initialize Adam optimizer: $optimizer = Adam(model.parameters())$
    Initialize learning rate scheduler: $scheduler = StepLR(optimizer)$
    for $epoch = 1, 2, \ldots, E$ **do**
        for $batch = 1, 2, \ldots, TD$ **do**
            Normalize targets: $y = normalize(y)$
            Predict binding energy: $\hat{y} = model(batch)$
            Calculate loss: $l = loss(y, \hat{y})$
            Backward pass: $l.backward()$
            Optimizer step: $optimizer.step()$
            if $epoch\%V == 0$ **then**
                Model in evaluation mode: $model.eval()$
                for $batch = 1, 2, \ldots, VD$ **do**
                    Normalize targets: $y = normalize(y)$
                    Predict binding energy: $\hat{y} = model(batch)$
                    Calculate loss: $l = loss(y, \hat{y})$
                    Apply exponential smoothing: $l = l * 0.9 + l_{-1} * 0.1$
                    Scheduler step: $scheduler.step(l)$
                end for
            end if
        end for
    end for
end for

5.4 Test Loop

Algorithm 2 MPNN Testing Loop

Initialize size of ensemble: T
Initialize size of batch: B
Initialize data sets: $Testd$,
initialize training data loader: $TestD = Dataloader(B, Testd)$
for $model = 1, 2, \ldots, T$ **do**
    Initialize target list: y_l
    Initialize prediction list: $\hat{y}_l$
    for $batch = 1, 2, \ldots, TestD$ **do**
        Normalize targets: $y = normalize(y)$
        Predict binding energy: $\hat{y} = model(batch)$
        Calculate loss: $l = loss(y, \hat{y})$
        Append target to list: y_l
        Append prediction to list: $\hat{y}_l$
    end for
    Save predictions and targets to file
    Save model to file
end for

5.5 Modelling Hyperparameters

Generally, two subsets of hyperparameters exists, those relevant to the less sophisticated set of ensemble models (titled MPNN64), and those relevant to the more sophisticated ensemble models (titled MPNN128). The table below1, details shared and non-shared model hyperparameters, as well as highlighting the parameters, which are consistent with the PAINN architecture described in [7] with a star (*).

5.5.1 Hyperparameter selection

Table 1: Modelling hyperparameters

Model Hyperparameters	***MPNN64***	***MPNN128***	***Unit***
Shared			
Number of physical dimensions*	3		Dimensions
Number of Message Passing Rounds*	5		Rounds
Patience*	5		Validation steps
Weight Decay*	0.01		N/A
Learning Rate Decay*	0.5		N/A
Exponential Smoothing for Validation*	0.9		N/A
Radial Basis Parameter*	20		N/A
Learning Rate	0.001		N/A
Cutoff Distance	4		Ångstrøm
Not shared			
State dimension size	64	128	Dimensions

An explanation of the individual hyperparameters influence on the model, and a justification for selection of the above values, can be be found in the appendix section10.1.

5.6 Experimental Hyperparameters

The experimental hyperparameters defining the implementation of the above model setting, can be found in table below2.

Table 2: Experimental Hyperparameters

Experimental Hyperparameters	***Value***	***Unit***
Number of molecules in Data Set	695	Molecules
Training Split	0.8	N/A
Validation Split	0.1	N/A
Test Split	0.1	N/A
Ensemble Size	5	Models
Initial number of Epochs	200	Epochs
Validation Index	5	Epochs
Model Saving Interval	0.01	N/A
Batch Size	5	Molecules

An in explanation of the selection of experiment hyperparameters and justification, be found in the appendix section10.2.

Table 4: Cloud Job Parameters

Cloud Job Parameters	***MPNN128***	***MPNN64***
Queue	**gpuv100**	**gpua100**
Number of cores	8	8
Memory/Cores	5 gb	5 gb
Number of hosts	1	1

5.7 Software tools and Hardware

The projects execution were developed in Python 3.10.9, with heavy emphasis on Pytorch, Numpy and Pandas, supported by few shell scripts for cloud job definitions. A full list of packages, and their versions utilized in the experiment, can be seen in appendix10.3 The initial datastructures and pipeline were inspired by course-material made by Mikkel Nørgaard Schmidt. The hardware utilized for the final experimental setup, were two two types of GPUs, belonging to the High Performance Computing (HPC) cluster at the Technical University of Denmark (DTU). The two queues utilized were 'gpua100' and 'gpuv100'. For further details on the hardware, please refer to the following reference:[18]. Total computation time in the cloud was three days, in order to produce the trained ensemble of ten individual models.

5.8 Reproduceability

For reviewing and reproduceability purposes, the following github link stores the latest version of the code: `https://github.com/Lohmann94/head`, which was utilized in the experiment. The experiment can be reproduced with the following seed-values3, which can be found for individual models:

Table 3: Model seeds for reproduction

MPNN128 Ensemble:		**MPNN64 Ensemble:**	
Model	***Seed***	***Model***	***Seed***
MPNN128_1	49	**MPNN64_1**	90
MPNN128_2	10	**MPNN64_2**	52
MPNN128_3	100	**MPNN64_3**	7
MPNN128_4	20	**MPNN64_4**	9
MPNN128_5	30	**MPNN64_5**	87

The cloud-job configuration variables for reproducing with the described performance, can be found in the below table4:

6 Data

6.1 Cross Coupling Catalysts

The data set of interest consists of 7.054 optimized geometries of compounds being candidate structures in oxidative addition catalystic process. The optimized geometries will have a binding energy associated with it, that dictates the net energy produced by the oxidative addition of a specific transition metal[13], which is the target of our modelling task. The original papers set out to further select 557 catalyst candidates which are within a predefined thermodynamic window, and a further selection of candidates based on their pricepoint per mol.

The molecular compounds are represented as graph structures of nodes and edges. The nodes constitute atoms, and the edges molecular connections between atoms. The representation will further consist of Cartesian coordinates provided in the data set, fixing the individual nodes in three dimensional space. This also provides the data set with the possibility of deriving distances between the nodes, or the length of edges, which are crucial to the modelling efforts.

The number of number of nodes in the graphs, range from a minimum of 5, a mean of 52.51, to a maximum of 123 nodes. A bar plot of the number of graphs in various buckets of node-counts, can be seen below5.

Figure 5: Bar plot of number of nodes per graph

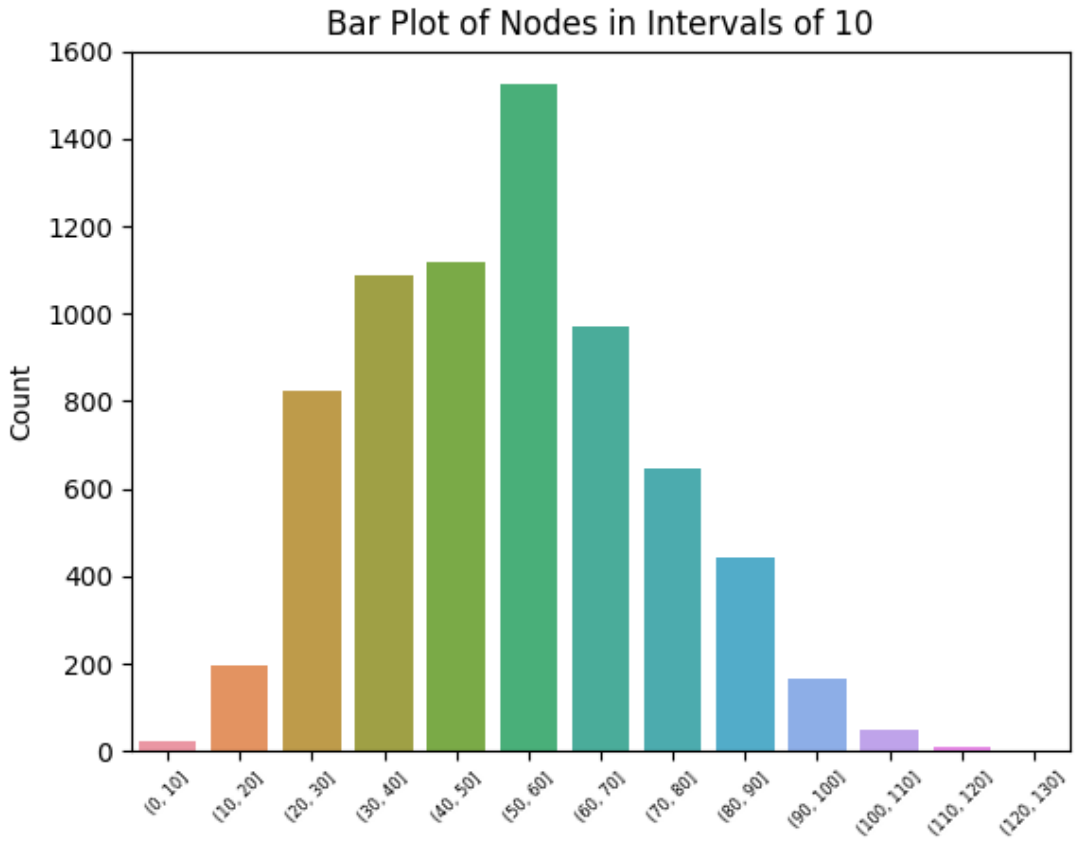

The atom distribution of the graphs a constituted by 13 unique atoms being:

- H: Hydrogen
- C: Carbon
- N: Nitrogen
- P: Phosphorus
- O: Oxygen
- Cl: Chlorine
- Pd: Palladium
- F: Fluorine
- Au: Gold
- Cu: Copper
- Ag: Silver
- Pt: Platinum

- Ni: Nickel

The distribution of the above atoms, can be seen in a Pareto graph below6. The distribution is mainly made up by hydrogen and carbon, those two being 90.6 percent of the atom-representation combined. The next highest contributor is nitrogen, only representing 3,4 percent of the atoms. The remaining atoms constitute 6 percent of the atom representation in the data set.

Figure 6: Pareto plot of atom distribution in data set

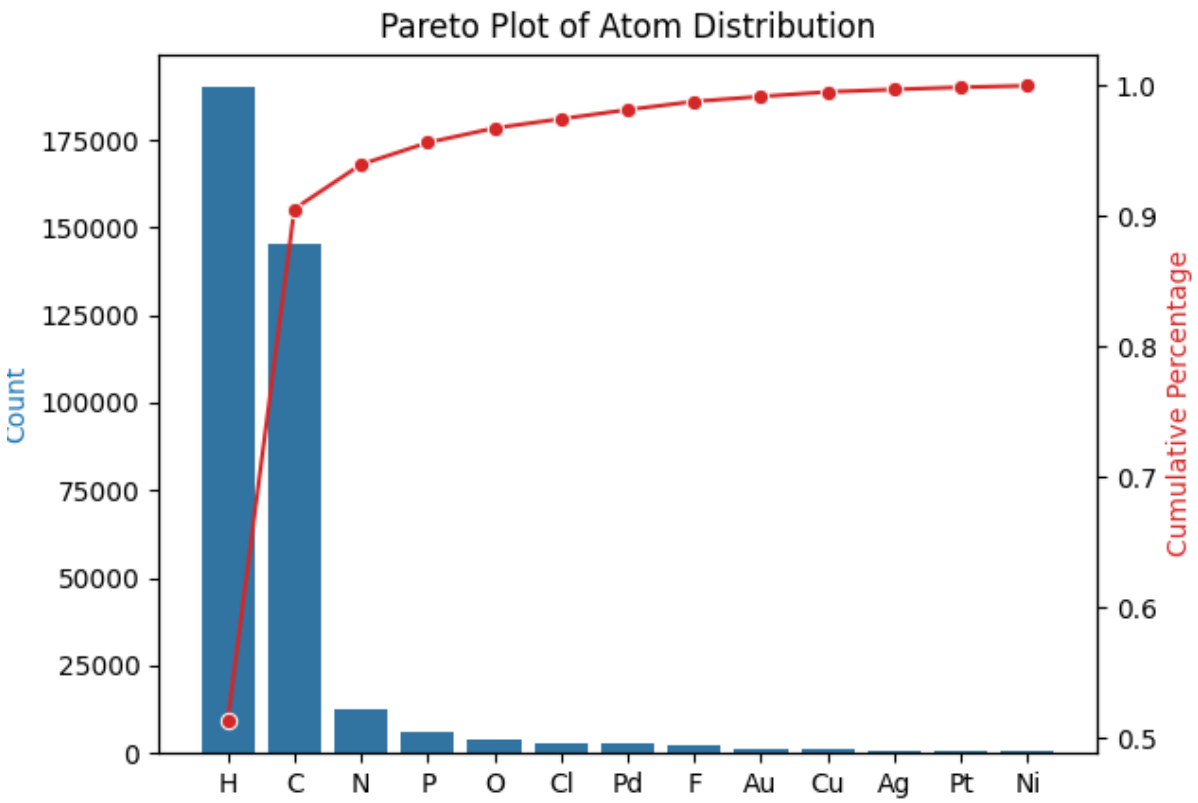

The additive part of the catalyst process, are selected transition metals, namely:

- Pd: Palladium
- Au: Gold
- Cu: Copper
- Ag: Silver
- Pt: Platinum
- Ni: Nickel

The data set consists of the following distribution of the above transition metals, below can be seen a pareto similar to further above, but now show the distribution of transition metals in the data set7.

Figure 7: Pareto plot of transition metal distribution in data set

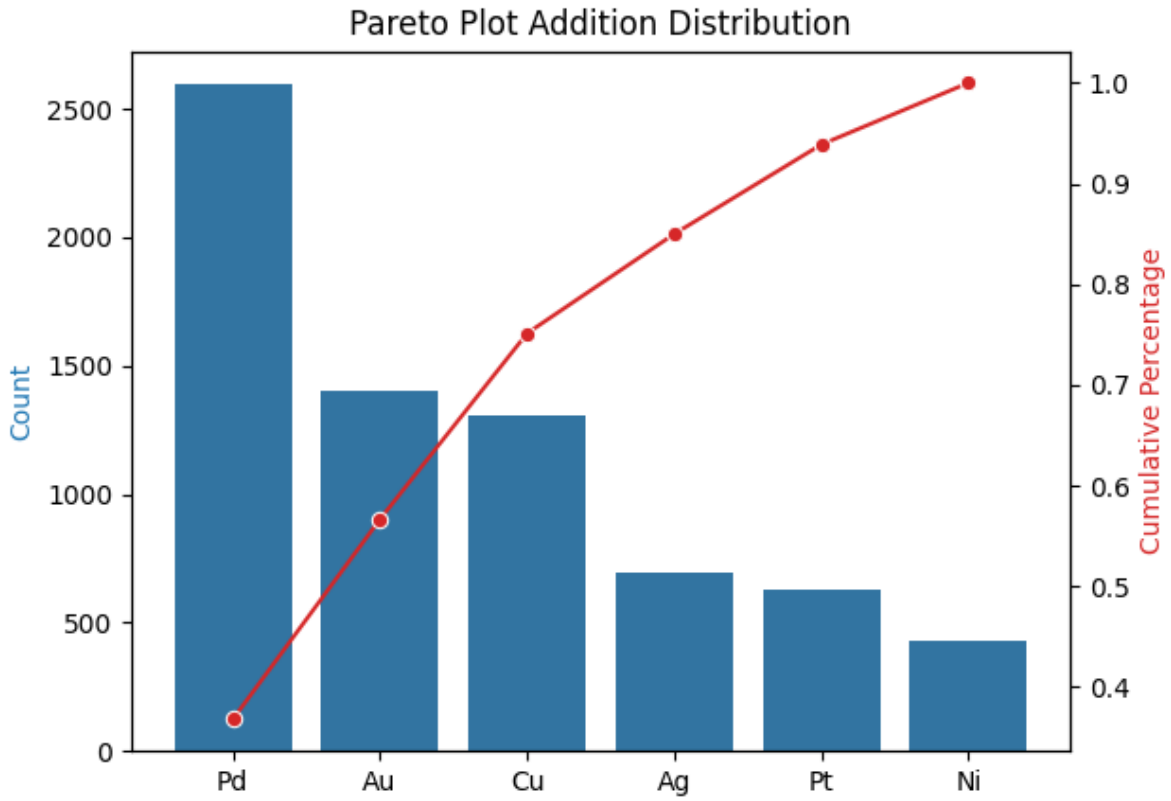

The distribution is mainly comprised of Palladium and Gold, standing for 57 percent of the transition metals in the data set.

The catalyst process can be both exothermic and endothermic, represented in either a positive net binding energy as a target, or a negative net binding energy as a target for the regression task. The regression targets range from a minimum of -80.82 being endothermic, to 61.49 being exothermic, where the mean is placed at -18.62. A bar plot with buckets of ten, of the distribution of targets can be seen below8.

Figure 8: Bar plot of binding energy distribution in targets

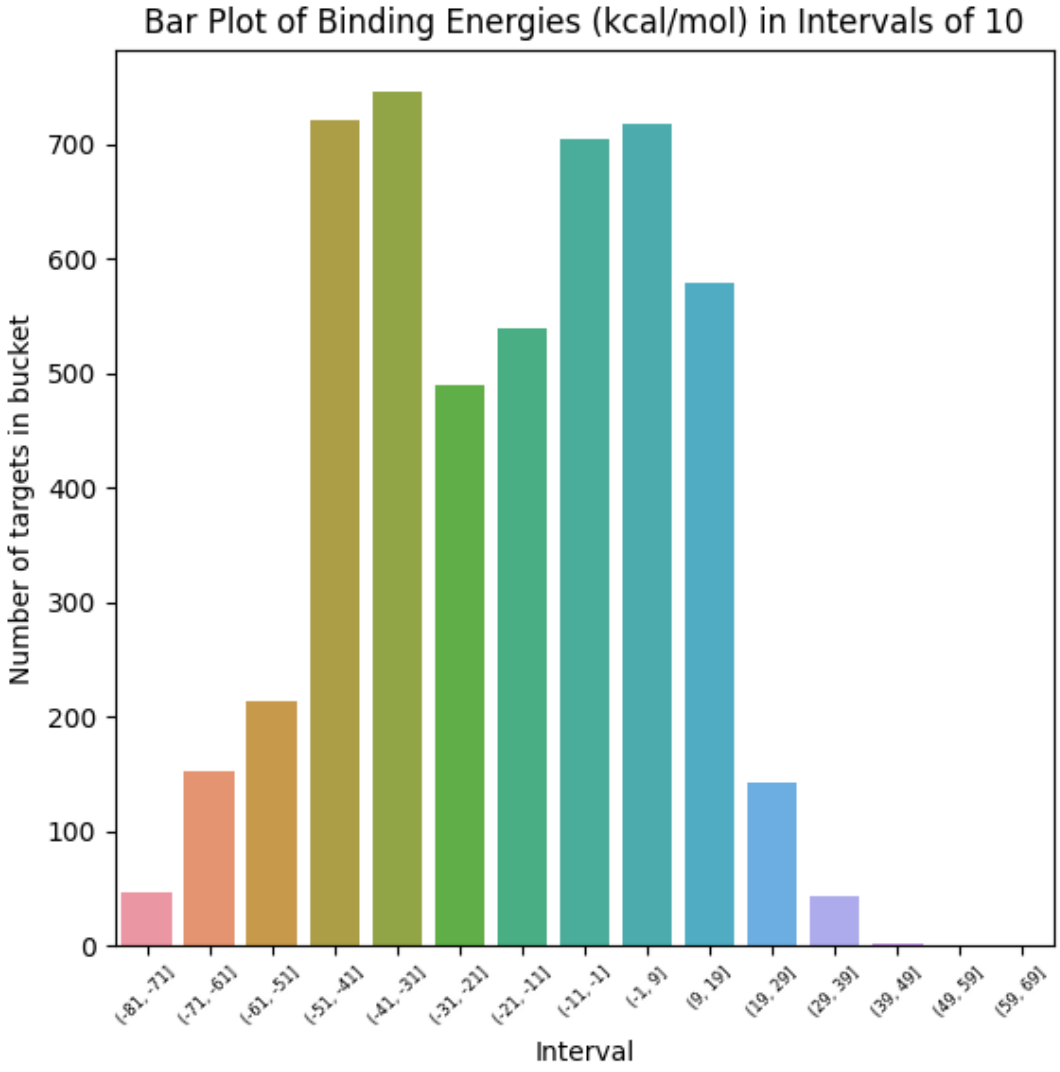

The edge-wise distances between nodes, measured in ångstrom, are crucial to the modelling task, since a model-parameter called 'r-cut', defines a cutoff limit from which edges with a distance lower than the cutoff are defined as neighbours of a given node, and those above as non-neighbours. The neighbours goes are allowed a higher model influence, and therefore understanding where to set the cutoff, is a crucial hyperparameter. The distances of the full data set is intractable to compute locally, so a subset of 50 randomly chosen graphs and their edge-wise distances are plotted as a representation of the full data set9. As we can see in the plot, most distances are covered by the interval 0 to 7, at 64 percent, and only 20 percent of distances lie in the interval above 8.5.

Figure 9: Pareto plot of Distances between edges from 50 graphs

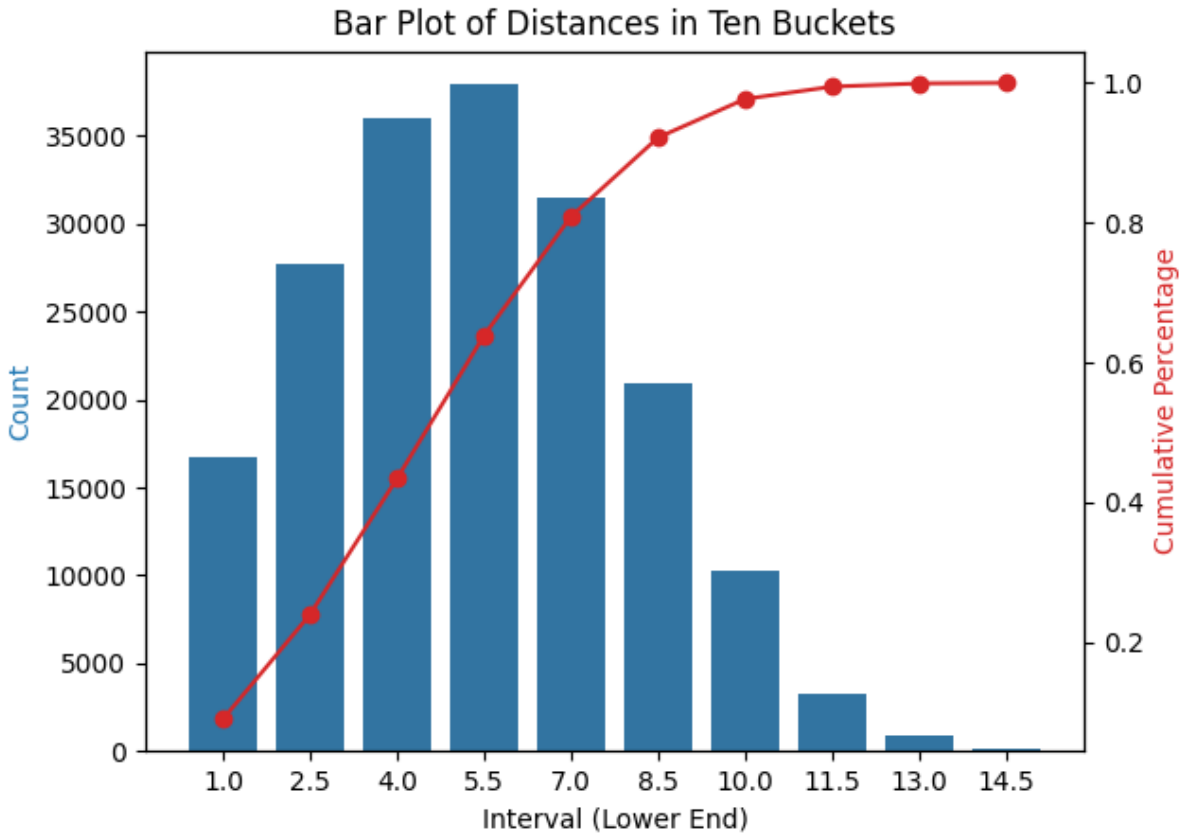

In a chemistry context, it is argued that a large portion in the variance in binding energy, can be explained by local interactions among atoms[7]. So even though a high degree of information lies beyond cutoff limits of i.e four or five, then information might not be crucial to the prediction in energy we are trying to make.

The modelling task will take in a given molecular structure, and produce a regression metric, trying to predict the associated binding energy from the oxidative addition in the unit kcal/mol. Further more, the regression efforts will be put in an ensemble context of a number of structurally similar models, producing a mean and a variance over the predicted regression metric from the ensemble.

6.2 Data Privacy- and Quality-issues

Due to the data sources being publicly available for download, under the creative commons attribution 4.0 license, the implementation and storage of the data, has been chosen to support all project activities in the most convenient way. Specifically that mean local and cloud storage, without password protection or encryption of the raw data.

The field of chemistry, that this study supports computationally, provide research which are used

within the life-science industry for drug-discovery among other fields.

With this in mind, sourcing of the data set needs to be carefully handled, taking into account potential end-user risks of promoting various molecules and processes through research, at some point in the process before consumption. The sourcing of the Cross-Coupling data set, is partly transparent. The initial data set is comprised of 25.116 graph structures, and was sourced through generating options based on 6 transition metals, mentioned above, and 91 ligands. This generation process was made by combining all possible combinations of the six transition metals and the 91 ligands, applying a filter for redundant chemical properties to reach the initial 25.116 size data set[13]. The reduction in data set size to the 7.054, was done by training a model to predict a chemical descriptor value relating to certain energy-levels, and then selecting these 7.054 molecules and transition metals based on that. No apparent precaution towards end-user complications are mentioned, and should therefore be applied further down stream of the research efforts within this field.

7 Results

8 Discussion

9 Conclusion

References

[1] J. Busk, P. B. Jørgensen, A. Bhowmik, M. N. Schmidt, O. Winther, and T. Vegge, "Calibrated uncertainty for molecular property prediction using ensembles of message passing neural networks," *Machine Learning: Science and Technology*, vol. 3, 7 2021. [Online]. Available: https://arxiv.org/abs/2107.06068v2

[2] J. Behler, "Atom-centered symmetry functions for constructing high-dimensional neural network potentials," *Journal of Chemical Physics*, vol. 134, p. 74106, 2 2011. [Online]. Available: /aip/jcp/article/134/7/074106/954787/Atom-centered-symmetry-functions-for-constructing

[3] J. Gasteiger, J. Groß, and S. Günnemann, "Directional message passing for molecular graphs," *8th International Conference on Learning Representations, ICLR 2020*, 3 2020. [Online]. Available: https://arxiv.org/abs/2003.03123v2

[4] K. Atz, F. Grisoni, and G. Schneider, "Geometric deep learning on molecular representations," *Nature Machine Intelligence*, vol. 3, pp. 1023–1032, 12 2021.

[5] O. T. Unke, M. Bogojeski, M. Gastegger, M. Geiger, T. Smidt, and K. R. Müller, "Se(3)-equivariant prediction of molecular wavefunctions and electronic densities," *Advances in Neural Information Processing Systems*, vol. 18, pp. 14 434–14 447, 6 2021. [Online]. Available: https://arxiv.org/abs/2106.02347v2

[6] S. Zhang, Y. Liu, and L. Xie, "Molecular mechanics-driven graph neural network with multiplex graph for molecular structures," 11 2020. [Online]. Available: https://arxiv.org/abs/2011.07457v1

[7] K. T. Schütt, O. T. Unke, and M. Gastegger, "Equivariant message passing for the prediction of tensorial properties and molecular spectra," *Proceedings of Machine Learning Research*, vol. 139, pp. 9377–9388, 2 2021. [Online]. Available: https://arxiv.org/abs/2102.03150v4

[8] J. Zhou, G. Cui, S. Hu, Z. Zhang, C. Yang, Z. Liu, L. Wang, C. Li, and M. Sun, "Graph neural networks: A review of methods and applications," *AI Open*, vol. 1, pp. 57–81, 12 2018. [Online]. Available: https://arxiv.org/abs/1812.08434v6

[9] H. Song, T. Diethe, M. Kull, and P. Flach, "Distribution calibration for regression," *36th International Conference on Machine Learning, ICML 2019*, vol. 2019-June, pp. 10 347–10 356, 5 2019. [Online]. Available: https://arxiv.org/abs/1905.06023v1

[10] E. Hüllermeier and W. Waegeman, "Aleatoric and epistemic uncertainty in machine learning: an introduction to concepts and methods," *Machine Learning*, vol. 110, pp. 457–506, 3 2021.

[11] G. Scalia, C. A. Grambow, B. Pernici, Y. P. Li, and W. H. Green, “Evaluating scalable uncertainty estimation methods for dnn-based molecular property prediction,” *Journal of Chemical Information and Modeling*, vol. 60, pp. 2697–2717, 10 2019. [Online]. Available: https://arxiv.org/abs/1910.03127v1

[12] T. Pearce, F. Leibfried, A. Brintrup, M. Zaki, and A. Neely, “Uncertainty in neural networks: Approximately bayesian ensembling,” *Proceedings of Machine Learning Research*, vol. 108, pp. 234–244, 10 2018. [Online]. Available: https://arxiv.org/abs/1810.05546v5

[13] B. Meyer, B. Sawatlon, S. Heinen, O. A. V. Lilienfeld, and C. Corminboeuf, “Machine learning meets volcano plots: Computational discovery of cross-coupling catalysts,” *Chemical Science*, vol. 9, pp. 7069–7077, 2018.

[14] B. Lakshminarayanan, A. Pritzel, and C. Blundell, “Simple and scalable predictive uncertainty estimation using deep ensembles,” *Advances in Neural Information Processing Systems*, vol. 2017-December, pp. 6403–6414, 12 2016. [Online]. Available: https://arxiv.org/abs/1612.01474v3

[15] K. Tran, W. Neiswanger, J. Yoon, Q. Zhang, E. Xing, and Z. W. Ulissi, “Methods for comparing uncertainty quantifications for material property predictions,” *Machine Learning: Science and Technology*, vol. 1, 12 2019. [Online]. Available: https://arxiv.org/abs/1912.10066v2

[16] “The radial basis function kernel.”

[17] K. Schütt, P.-J. Kindermans, H. E. S. Felix, S. Chmiela, A. Tkatchenko, and K.-R. Müller, “Schnet: A continuous-filter convolutional neural network for modeling quantum interactions,” *Advances in Neural Information Processing Systems*, vol. 30, 2017. [Online]. Available: www.quantum-machine.org.

[18] “Using gpus under lsf10.” [Online]. Available: https://www.hpc.dtu.dk/?page_id=2759

10 Appendix

10.1 Appendix A

10.2 Appendix B

10.3 Appendix C

Two lists of main packages, and their versions vital to local development and cloud execution. First the local development packages10.3:

- Python 3.10.9
- Pytorch 2.0.1+cu118
- numpy 1.23.5
- pandas 1.5.2
- matplotlib 3.7.0
- tqdm 4.65.0
- python-dotenv 1.0.0

And for cloud execution10.3:

- Python 3.9.14
- Pytorch 2.1.0+cu118
- numpy 1.23.5
- pandas 1.5.2
- scipy 1.9.1bstat
- tqdm 4.66.1